AFRL-SN-WP-TP-2006-107

ACCELERATION OF DIELECTRIC CHARGING IN RF MEMS CAPACITIVE SWITCHES (PREPRINT)

Xiaobin Yuan, James C.M. Hwang, David I. Forehand, and Charles L. Goldsmith

MARCH 2006

Approved for public release; distribution is unlimited.

STINFO COPY

SENSORS DIRECTORATE
AIR FORCE RESEARCH LABORATORY
AIR FORCE MATERIEL COMMAND
WRIGHT-PATTERSON AIR FORCE BASE, OH 45433-7320

NOTICE AND SIGNATURE PAGE

AFRL-SN-WP-TP-2006-107 HAS BEEN REVIEWED AND IS APPROVED FOR PUBLICATION IN ACCORDANCE WITH ASSIGNED DISTRIBUTION STATEMENT.

//Signature//

JOHN L. EBEL
Devices for Sensing Branch
Aerospace Components Division

//Signature//

KENICHI NAKANO, Chief
Devices for Sensing Branch
Aerospace Components Division

//Signature//

TODD A. KASTLE, Chief
Aerospace Components Division
Sensors Directorate

REPORT DOCUMENTATION PAGE

Form Approved
OMB No. 0704-0188

1. REPORT DATE *(DD-MM-YY)*	2. REPORT TYPE	3. DATES COVERED *(From - To)*
March 2006	Journal Article Preprint	08/23/2003 – 03/01/2006

4. TITLE AND SUBTITLE
ACCELERATION OF DIELECTRIC CHARGING IN RF MEMS CAPACITIVE SWITCHES (PREPRINT)

5a. CONTRACT NUMBER
F33615-03-C-7003

5b. GRANT NUMBER

5c. PROGRAM ELEMENT NUMBER
63739E

6. AUTHOR(S)
Xiaobin Yuan, James C.M. Hwang, David I. Forehand, and Charles L. Goldsmith

5d. PROJECT NUMBER
ARPS

5e. TASK NUMBER
ND

5f. WORK UNIT NUMBER
AN

7. PERFORMING ORGANIZATION NAME(S) AND ADDRESS(ES)

MEMtronics Corporation
3000 Custer Road, Suite 270-400
Plano, TX 75075

8. PERFORMING ORGANIZATION REPORT NUMBER

9. SPONSORING/MONITORING AGENCY NAME(S) AND ADDRESS(ES)

Sensors Directorate
Air Force Research Laboratory
Air Force Materiel Command
Wright-Patterson Air Force Base, OH 45433-7320

10. SPONSORING/MONITORING AGENCY ACRONYM(S)
AFRL-SN-WP

11. SPONSORING/MONITORING AGENCY REPORT NUMBER(S)
AFRL-SN-WP-TP-2006-107

12. DISTRIBUTION/AVAILABILITY STATEMENT
Approved for public release; distribution is unlimited.

13. SUPPLEMENTARY NOTES
PAO Case Number: AFRL/WS 06-0992, 17 Apr 2006. Report contains color.

This work has been submitted to IEEE for publication in *IEEE Transactions on Microwave Theory and Techniques.*

14. ABSTRACT

To design and validate accelerated life tests of RF MEMS capacitive switches, acceleration factors of charging effects in switch dielectric were quantitatively characterized.

From the measured charging and discharging transient currents at different temperatures and control voltages, densities and time constants of dielectric traps were extracted. A charging model was constructed to predict the amount of charge injected into the dielectric and the corresponding shift in actuation voltage under different acceleration factors such as temperature, peak voltage, duty factor, and frequency of the control waveform. Agreement was obtained between the model prediction and experimental data. It was found that temperature, peak voltage, and duty factor were critical acceleration factors for dielectric-charging effects whereas frequency had little effect on charging.

15. SUBJECT TERMS
RF MEMS, Dielectric Charging, low loss

16. SECURITY CLASSIFICATION OF:			17. LIMITATION OF ABSTRACT:	18. NUMBER OF PAGES	19a. NAME OF RESPONSIBLE PERSON (Monitor)
a. REPORT	b. ABSTRACT	c. THIS PAGE			John L. Ebel
Unclassified	Unclassified	Unclassified	SAR	14	19b. TELEPHONE NUMBER *(Include Area Code)* N/A

Standard Form 298 (Rev. 8-98)
Prescribed by ANSI Std. Z39-18

Acceleration of Dielectric Charging in RF MEMS Capacitive Switches

Xiaobin Yuan, *Student Member, IEEE,* Zhen Peng, James C. M. Hwang, *Fellow, IEEE,* David Forehand, *Member, IEEE,* and Charles L. Goldsmith, *Senior Member, IEEE*

***Abstract*—To design and validate accelerated life tests of RF MEMS capacitive switches, acceleration factors of charging effects in switch dielectric were quantitatively characterized. From the measured charging and discharging transient currents at different temperatures and control voltages, densities and time constants of dielectric traps were extracted. A charging model was constructed to predict the amount of charge injected into the dielectric and the corresponding shift in actuation voltage under different acceleration factors such as temperature, peak voltage, duty factor, and frequency of the control waveform. Agreement was obtained between the model prediction and experimental data. It was found that temperature, peak voltage, and duty factor were critical acceleration factors for dielectric-charging effects whereas frequency had little effect on charging.**

***Index Terms*—Charging, dielectric, lifetime, MEMS, RF, reliability, switch, trap, temperature acceleration, accelerated life test.**

I. Introduction

RF MEMS is an emerging technology for low-loss switch, phase shifter, and reconfigurable network applications [1]-[4]. However, commercialization of RF MEMS devices is hindered by the need for continuing improvements in reliability and packaging. In particular, lifetimes of electrostatically actuated RF MEMS capacitive switches are limited by dielectric-charging effects [5]. The dielectric is typically low-temperature deposited silicon dioxide or nitride with a high density (10^{18} cm^{-3}) of traps associated with silicon dangling bonds. During switch operation, the electric field across the dielectric can be higher than 10^6 V/cm causing electrons to be injected into the dielectric and become trapped. With repeated operation, charge gradually builds up in the dielectric, modifying the electrostatic force on the movable membrane resulting in actuation-voltage shift and/or stiction [6].

To date, dielectric-charging effects in RF MEMS devices have been studied by different research groups [5]-[9] with a qualitative charging model proposed [9]. In comparison, we have proposed a quantitative charging model to predict charge injection and actuation-voltage shift at room temperature [10]. However, for switch applications in harsh environment (e. g., over the military temperature range of −55 to 125°C), temperature acceleration of charging needs to be modeled as well. Moreover, acceleration of charging effects under different control waveforms has not been characterized and modeled in detail. Using the transient current measurement technique developed in [10], temperature acceleration of the charging effects was first reported in [11]. This paper expands on [11] to include characterization and modeling of charging under control waveforms of different peak voltages, duty factors, and frequencies, as well as under dual pulses. It was found that temperature, duty factor, and peak voltage were critical acceleration factors for charging effects whereas frequency had little effect on charging. The significantly reduced charging effects under dual-pulse waveforms were also modeled correctly. Therefore, for RF MEMS capacitive switches that fail mainly due to dielectric charging, the present model can be used to design control waveforms that can either prolong lifetime or accelerate failure.

Manuscript submitted on March 30, 2006. Work was partially supported by the US Air Force Research Laboratory under Contract No. F33615-03-C-7003. The contract was funded by the US Defense Advanced Research Projects Agency under the Harsh Environment, Robust Micromachined Technology (HERMIT) program.

X. Yuan, Z. Peng, and J. C. M. Hwang are with Lehigh University, Bethlehem, PA 18015 USA. J. C. M. Hwang can be contacted at +1 (610) 758-5104 or jh00@lehigh.edu.

D. Forehand and C. Goldsmith are with MEMtronics Corp., Plano, TX 75075

II. Experimental

A. Device Structure

The device used in this study is a state-of-the-art metal-dielectric-metal RF MEMS capacitive switch fabricated on a glass substrate. The dielectric is sputtered silicon dioxide with a thickness of 0.25 μm and a dielectric constant of 4.5. The top electrode is a 0.3-μm-thick flexible aluminum membrane that is grounded. The bottom chromium/gold electrode serves as the center conductor of a 50 Ω coplanar waveguide for the RF signal. The actuation voltage of the switch is approximately 22 V. Without any electrostatic force, the membrane is normally suspended in air 2.5 μm above the dielectric. Control voltage with a magnitude of 25-35 V is applied to the bottom electrode, which brings the membrane in contact with the dielectric thus forming a 120 μm x 80 μm capacitor to shunt the RF signal to ground. When the control voltage is reduced to below the release voltage of 8 V, the membrane springs back to its fully suspended position, resulting in little capacitive load to the RF signal. The switch has low insertion loss (0.06 dB) and reasonable isolation (15 dB) at 35 GHz. The switching time is less than 10 μs. Details of the design, fabrication and performance of the switch were reported in [1].

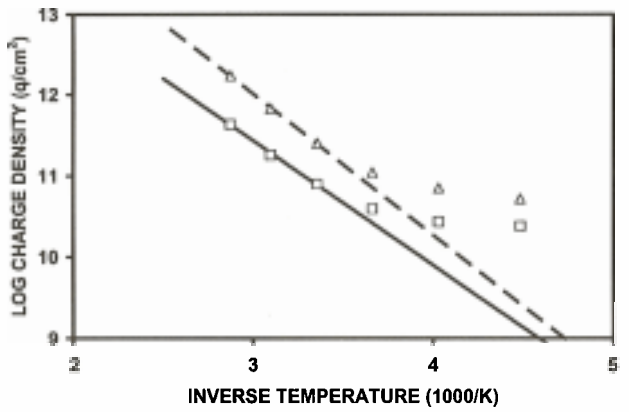

Fig. 1. Comparison of extracted and fitted temperature dependence of steady-state charge densities. Extracted charge densities are for (□) trap 1 and (Δ) trap 2 at −50, −25, 0, 25, 50, and 75°C. Fitted charge densities are for (—) trap 1 and (---) trap 2. The control voltage is −30 V.

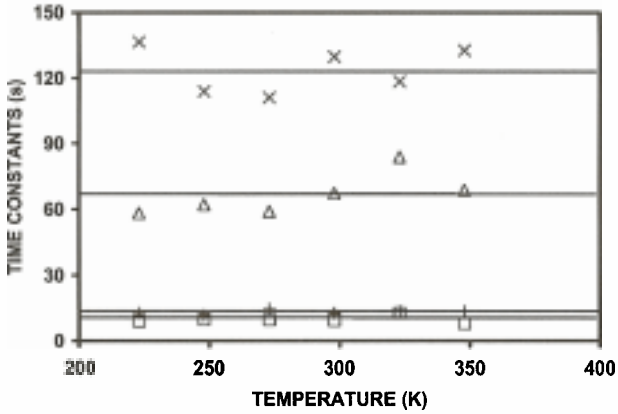

Fig. 2. Extracted (□) trap 1 charging, (+) trap 1 discharging, (Δ) trap 2 charging, and (x) trap 2 discharging time constants at −50, −25, 0, 25, 50, and 75°C. The control voltage is −30 V. Solid lines indicate the average values of the time constants over temperature.

B. Transient Current Measurements

In order to extract the temperature-dependent charging model, charging and discharging transient currents were measured under different temperatures on large (500 μm x 500 μm) metal-insulator-metal (MIM) capacitors with the same electrode and dielectric material as the switch. A precision semiconductor parameter analyzer (Agilent 4156C) was used to force a −30 V pulse on the bottom electrode of the MIM capacitor while sensing the transient current. Well-guarded probe station and probes were used to suppress the capacitive and leakage currents in the measurement path, thus extending the transient current measurement range below pA level.

When a voltage pulse is applied to an MIM capacitor, the total current across the capacitor includes displacement current, trap charging current, and steady-state leakage current. Since the time constant for the displacement current is of the order of milliseconds, the transient currents measured in seconds comprise mainly trap charging currents. Similarly, transient currents measured after the voltage pulse is removed comprise mainly trap discharging currents. In this case, trap densities, and charging/discharging time constants can be extracted from the measured transient currents at different temperatures.

C. Accelerated Life Tests

Accelerated life tests were performed on real switches by using a time-domain switch characterization setup [6]. A 6 GHz, 10 dBm sinusoidal signal was applied to the switch input port together with the control voltage. The RF output was sensed by using a Narda 26.5 GHz diode detector. Both the control and output waveforms were monitored by using an oscilloscope. First, a 0 to −30 V saw-tooth control wave was applied to the bottom electrode of a pristine switch to sense the pre-stress actuation voltage. Next the switch was stressed by applying a square or dual-pulse stress wave for different time periods. After each stress period, another saw-tooth control wave was applied to the switch to sense the post-stress actuation voltage. This way, the actuation-voltage shift for each stress period can be determined. Peak voltage, duty factor, and frequency of the square stress wave were varied to investigate their acceleration effects on actuation-voltage shift. Comparison between square and dual-pulse waves was also made. Ultimate switch failure is defined by stiction, which occurs after the actuation voltage is shifted by approximately 8 V. This means that, when a negative control voltage is applied to the bottom electrode, the actuation voltage would shift from −22 to −14 V. With a release voltage of −8 V, a shift larger than 8 V will change the release voltage to 0 resulting in stiction [9].)

III. Temperature-Dependent Charging Model

The injected charge density in the dielectric can be modeled as [10]

$$Q = \sum_j Q_j [1 - \exp(-t_{on} / \tau_{CJ})] \exp(-t_{off} / \tau_{DJ}), \quad (1)$$

where Q_J is the steady-state charge density, τ_{CJ} and τ_{DJ} are the charging and discharging time constants of the *Jth* species of trap, t_{ON} and t_{OFF} are the on and off times of the switch corresponding to the charging and discharging times.

Assuming all traps are empty before applying the control voltage pulse, transient current after the voltage is turned on is

$$I_c = qA \frac{dQ}{dt} = qA \sum_j \frac{Q_j}{\tau_{CJ}} \exp(-t_{on} / \tau_{CJ}), \quad (2)$$

where q is the electron charge, and A is the surface area of the dielectric. Similarly, assuming the traps are all charged during the voltage pulse duration, transient current due to the discharging of the traps after removal of the voltage is

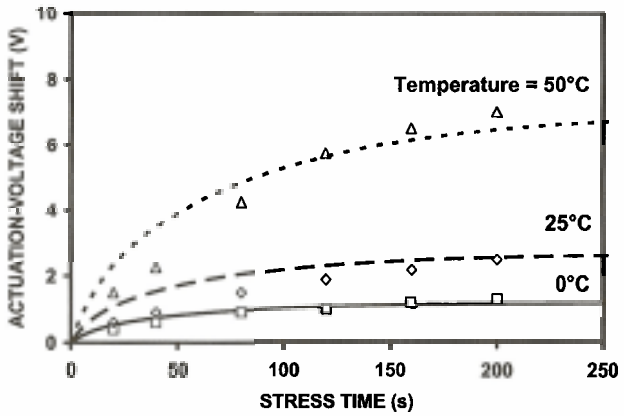

Fig. 3. Measured actuation-voltage shift at (□) 0, (◊) 25, and (Δ) 50°C vs. modeled actuation-voltage shift at (—) 0°C, (---) 25°C, and (···) 50°C. Measurement was taken after 20, 40, 80, 120, 160, and 200 s of −30 V stress on the bottom electrode of the switch.

$$I_D = qA\frac{dQ}{dt} = -qA\sum_j \frac{Q_{oj}}{\tau_{Dj}}\exp(-t_{ost}/\tau_{Dj}). \quad (3)$$

Charging model parameters (Q_J, τ_{CJ}, and τ_{DJ}) were extracted at different temperatures (−50, −25, 0, 25, 50, and 75°C) by fitting the measured transient currents under the −30 V control voltage with exponential functions of (2) and (3). Two exponential functions, representing two trap species, were found to give good fit.

As shown in Fig. 1, the extracted steady-state charge densities for trap 1 and trap 2 both increase with temperature.

Temperature dependence of the steady-state charge density for the *Jth* trap is modeled using the standard equation for a thermally activated process

$$Q_j = Q_{0j}\exp(-E_{Aj}/KT), \quad (4)$$

where E_A is the activation energy and Q_0 is a fitting parameter. By using (4), temperature dependence of the steady-state charge density was fitted well for temperatures above 0°C as shown in Fig. 1. For temperatures below 0°C, the data deviate from the fitted line indicating that a different process with a different set of E_A and Q_0 should be considered. However, charging is more critical above 0°C where not only the steady-state charge density is higher, but also the membrane is softer hence more prone to stiction. Since it is more critical for the model to be accurate above 0°C, to reduce the complexity of the model, only one set of E_A and Q_0 were used to describe the temperature dependence of the steady-state charge density as in (4).

While the steady-state charge densities are temperature dependent, the extracted charging and discharging time constants are relatively independent of temperature as shown in Fig. 2. Therefore, τ_C and τ_D were taken as the average of the time constants extracted under different temperatures.

From the measured charging and discharging transient currents on the MIM capacitor, charging model parameters were extracted for the −30 V control voltage using the above-described approach. The actuation-voltage shift due to dielectric charging can be expressed as

$$\Delta V = qhQ/\varepsilon_0\varepsilon_r, \quad (5)$$

where h is the distance between the bottom electrode and the trapped charge sheet, Q is the injected charge density predicted by the charging model (1), ε_0 is the permittivity of free space, and ε_r is the relative dielectric constant. Since h cannot be directly measured, the actuation-voltage shift for a certain stress period is predicted by the charging model (1), (4), and (5) with h optimized to give the best fit between model prediction and experimental data at all temperatures.

IV. Charging Under Temperature Stress

The temperature-dependent dielectric-charging effect was characterized by applying a constant (DC) stress voltage on the bottom electrode of the switch for different time periods while measuring the corresponding actuation-voltage shift. The −30 V stress voltage used in the experiment is sufficient to actuate the switch at all measurement temperatures (0, 25, and 50°C). The actuation voltage was shifted in the positive direction after the stress indicating injection of electrons from the bottom electrode into the dielectric at all temperatures. Fig. 3 shows the measured and modeled actuation-voltage shifts after different stress periods at different temperatures. The extracted temperature-dependent charging model compares reasonably well with the measured results. Both modeled and measured results suggest that increasing the operating temperature will accelerate charging resulting in larger actuation-voltage shifts. On the other hand, the spring constant and restoring force of the membrane decrease at elevated temperatures. Therefore, the switch is more prone to charge-induced stiction when temperature increases. Conversely, lowering the temperature will increase the membrane spring constant while reducing charge injection, which will render a longer switch lifetime.

V. Charging Under AC Stress

Switch lifetime has exhibited an exponential dependence on the control voltage [5], implying that either charge density or time constant is strongly dependent on control voltage. By measuring the transient charging/discharging currents under different control voltages, a voltage-dependent charging model was extracted at room temperature showing that the steady-state charge densities depend on the control voltage exponentially whereas time constants have no obvious voltage dependence [10]. Using the model, the amount of injected charge was calculated and compared with the measured data at room temperature under periodic (AC) control waveforms of

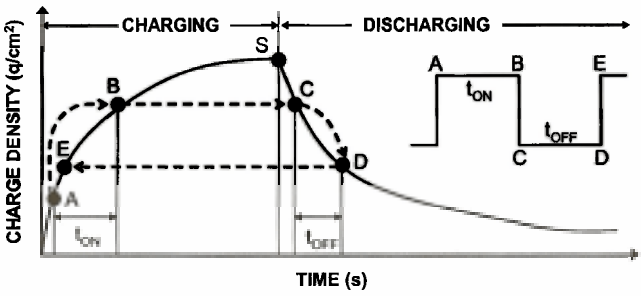

Fig. 4. Charging calculation under a square wave. t_{ON} and t_{OFF} are the on and off times of the switch. After one operating cycle, charge density increases from the initial state A to the end state E. Inset illustrates the applied square wave and the corresponding charging states.

different peak voltages, duty factors, and frequencies as well as under dual pulses.

A. Charging Calculation

Fig. 4 illustrates a charging curve that starts from the origin and ends in saturation (state S), which is followed by a discharging curve that falls exponentially as shown in the charging model (1). The charging and discharging curves are generated from the charging model equations and can be expressed as in the following:

$$Q = \sum_j Q_j [1 - \exp(-t_{ON} / \tau_{CJ})]; \quad (6)$$

$$Q = \sum_j Q_j \exp(-t_{OFF} / \tau_{DJ}). \quad (7)$$

where Q_J is the voltage-dependent steady-state charge density of the *Jth* species of trap, τ_{CJ} and τ_{DJ} are the corresponding charging and discharging time constants.

During real switch operation under a square wave, the charging state at the beginning of each operating cycle can be somewhere between empty and full, such as state A illustrated on the charging curve. After the switch is turned on, the charging state moves higher to state B during the on time of the switch. After the switch is turned off, the dielectric starts to discharge from state C on the discharging curve, which is mapped horizontally from state B of the charging curve. After certain off time, the dielectric is discharged to state D, which is then mapped back to state E on the charging curve to start the next operating cycle. Thus, the net effect of one operating cycle of the switch is to move the charging state from A to E. The charging/discharging model repeats in such a ratchet fashion until the desired number of cycles has been operated. To calculate charge injection under square waves, the model needs four input parameters: peak voltage, on time, off time, and number of cycles. Alternatively, on and off times can be specified in terms of frequency and duty factor of the waveform.

For a giving frequency, the on and off times within one operating cycle are determined by the duty factor. For the extreme case of a constant stress (duty factor = 100%), the

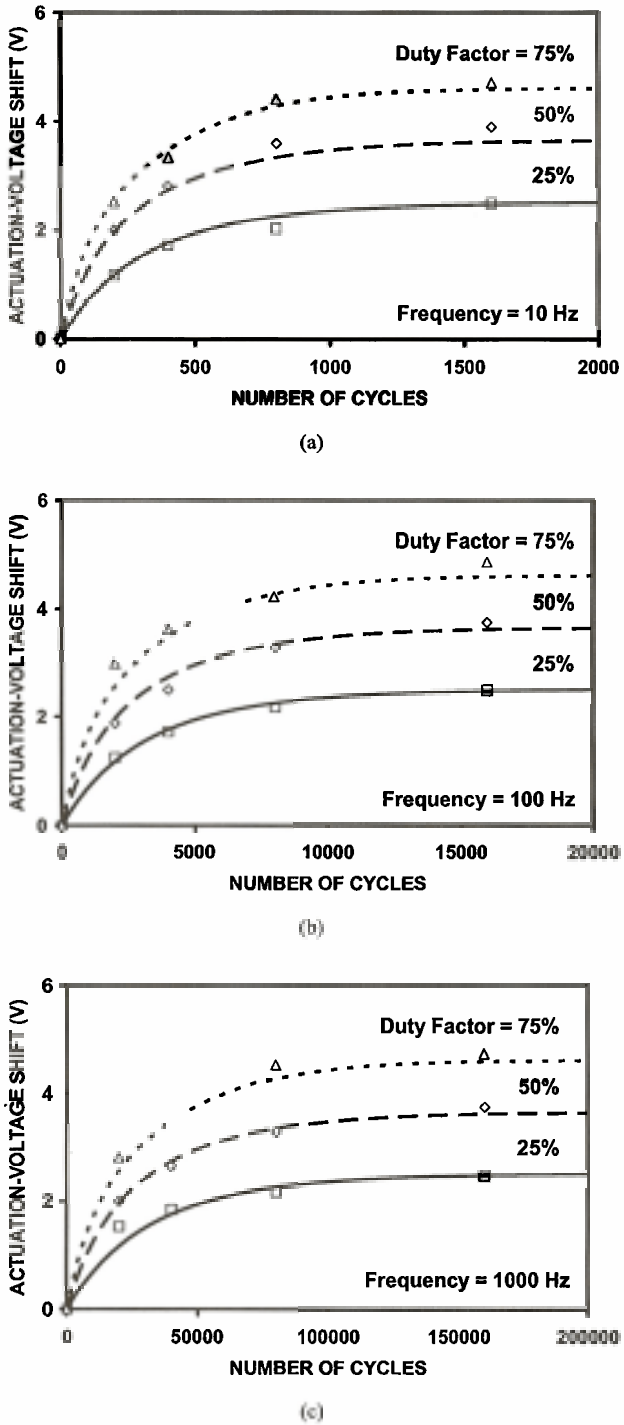

Fig. 5. Actuation-voltage shift as a function of operating cycles. The stress signal is a 0 to −30 V square wave at (a) 10, (b) 100 and (c) 1000 Hz. Modeled actuation-voltage shifts are for (—) 25%, (- - -) 50%, and (· · ·) 75% duty factors. Similarly, measured actuation-voltage shifts are for (□) 25%, (◊) 50%, and (Δ) 75% duty factors. Stress times (20, 40, 80, and 160 s) are the same for all three frequencies. Both modeled and measured data show that actuation-voltage shift is accelerated by duty factor, but not by frequency.

charge density will eventually reach a saturated value $\sum Q_J$ as indicated by state S in Fig. 4. For an extremely low duty factor

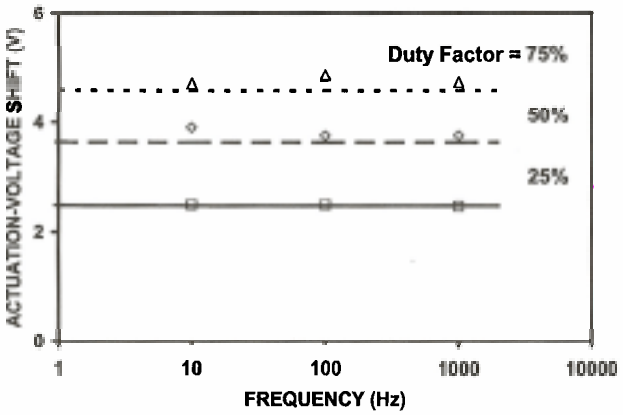

Fig. 6. Actuation-voltage shift as a function of stress signal frequency. The stress signal is a 0 to −30 V, 160 s long square wave. Modeled actuation-voltage shifts are for (—) 25%, (- - -) 50%, and (· · ·) 75% duty factors at all frequencies. Measured actuation-voltage shifts are for (□) 25%, (◊) 50%, and (Δ) 75% duty factors at 10, 100, and 1000 Hz. Both modeled and measured data show little frequency dependence.

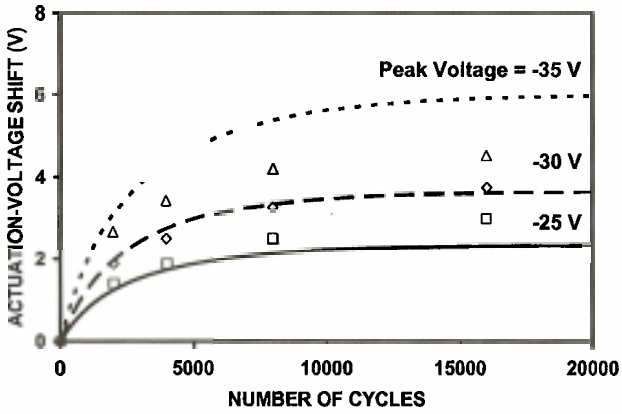

Fig. 7. Actuation-voltage shift as a function of operating cycles and square-wave peak voltages under a 100 Hz, 50% duty factor square wave. Modeled actuation-voltage shifts are for (—) −25, (- - -) −30, and (· · ·) −35 V peak voltages. Similarly, measured actuation-voltage shifts are for (□) −25 V, (◊) −30 V, and (Δ) −35 V peak voltages. Both modeled and measured data show that charge injection is accelerated by increasing peak voltage of the square wave.

such as 0.01%, the charge accumulated during the on time of the switch will be discharged almost completely during the off time; hence little charge will ever be accumulated. An intermediate duty factor, e. g., 50%, will cause the charge density to saturate at a value somewhere between 0 and $\sum Q_j$ when the charging and discharging processes are balanced. Initially, in a pristine switch charging is fast but discharging is slow. This builds up charge so that charging slows while discharging accelerates until charging and discharging are balanced. Thus, with the proper switch design and control waveform, it is possible to avoid switch failure even after charging or actuation-voltage shift saturates.

It has been suggested that charging is dependent on the total on time only and independent of off time, duty factor, or frequency. While this may be the case initially when charging is fast and discharging is slow, it may not be valid after significant charge is built up and significant discharging occurs during off time.

For reasons discussed above, the commonly quoted number of cycles before failure, due to its dependence on the detailed control waveform, is not a universal figure of merit for RF MEMS capacitive switches [9]. For a square wave with its peak voltage defined by the actuation voltage of the switch, frequency and duty factor must be specified for the quoted switch life cycles to be meaningful. Conversely, with the acceleration effects quantified through the present charging model, a fair comparison can be made between lifetimes measured under different frequencies and duty factors.

B. Duty-Factor Acceleration

Under a square control wave, the amount of charging within one operating cycle is determined by three parameters: peak voltage, duty factor, and frequency. We first investigate the effects of frequency and duty factor, while keeping the peak voltage constant. Specifically, the square wave used in the study has an on voltage of −30 V and an off voltage of 0. The actuation voltage of the pristine switch is approximately −22 V at room temperature. Therefore, peak voltage of −30 V ensures switch operation after significant actuation-voltage shift in either direction. A pristine switch was operated at three different frequencies: 10, 100, and 1000 Hz. Three duty factors were used at each frequency: 25%, 50%, and 75%.

After stressing a pristine switch with the 0 to −30 V square wave for a certain period, actuation voltage was shifted in the positive direction (less negative) indicating injection of electrons from the bottom electrode into the dielectric. By using (5) with an optimized h value, good fit was found between modeled and measured actuation-voltage shifts at all three frequencies and duty factors as shown in Fig. 5. Both modeled and measured data suggest that, for a fixed duty factor, dielectric charging and actuation-voltage shift depend strongly on the total stress time instead of the number of operating cycles. Notice that in Fig. 5 the total number of cycles, (a) 2000, (b) 20000, and (c) 200000, at the three frequencies correspond to the same total stress time of 200 s. Hence, within the frequency range of 10 to 1000 Hz, charge injection has no obvious dependence on the stress frequency as further illustrated in Fig. 6. This is consistent with the experimental results in [9]. On the other hand, increasing the square-wave duty factor accelerates dielectric charging and actuation-voltage shift at all frequencies as shown in Fig. 5 and 6.

C. Voltage Acceleration

It has been shown that increasing the peak voltage accelerates charge injection and shortens the switch lifetime [5]. We now analyze voltage acceleration of dielectric charging under a 100 Hz, 50% duty factor square wave with −25 V, −30 V, and −35 V peak voltages. Both modeled and measured data

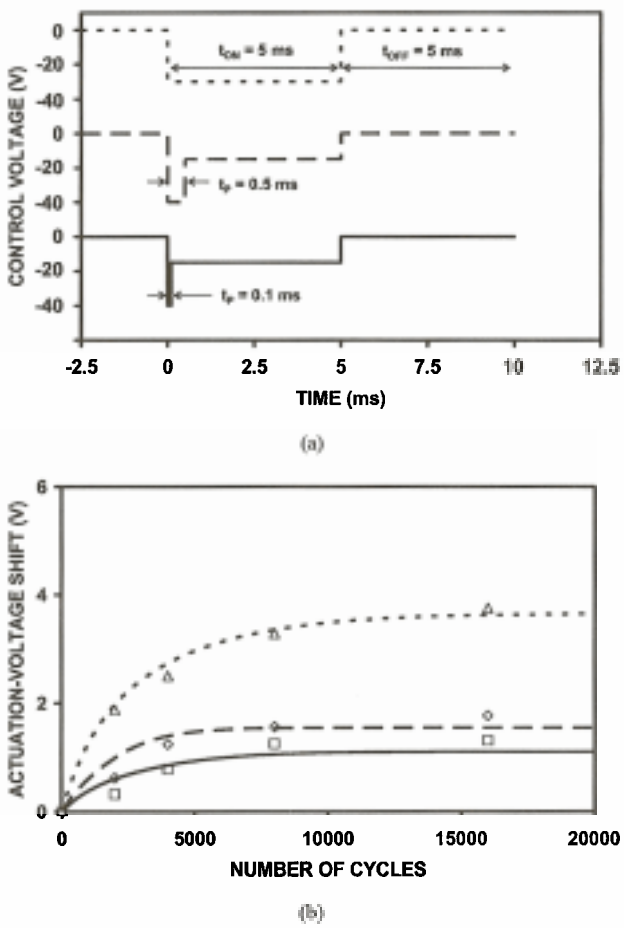

Fig. 8. (a) Control waveforms of (—) dual pulse with t_P = 0.1 ms, (- - -) dual pulse with t_P = 0.5 ms, and (· · ·) square wave with 50% duty factor. For the dual-pulse waves, pull-down voltage is −40 V and hold-down voltage is −15 V. The square wave is from 0 to −30 V. The frequency is 100 Hz in all three cases. (b) Actuation-voltage shift as a function of operating cycles. Modeled actuation-voltage shifts are for (—) dual pulse with t_P = 0.1 ms, (- - -) dual pulse with t_P = 0.5 ms, and (· · ·) square wave. Measured actuation-voltage shifts are for (□) dual pulse with t_P = 0.1 ms, (◊) dual pulse with t_P = 0.5 ms, and (Δ) square wave. Charge injection is minimized by using the dual-pulse waves instead of the square wave.

shown in Fig. 7 confirm that increasing the peak voltage accelerates dielectric charging hence actuation-voltage shift. Since the peak voltage affects steady-state charge densities but not charging/discharging time constants [10], similar voltage acceleration can be expected for other frequencies and duty factors.

D. Dual-Pulse Actuation

A dual-pulse waveform has been proposed to minimize charging [5]. The waveform comprises a short high-voltage pulse to quickly pull down the membrane and a low-voltage pulse to hold down the membrane for the remaining on time. Thus, for most of the on time the dielectric is subject to the low-voltage hold-down pulse and charging is minimized due to its exponential voltage dependence [10]. As illustrated in Fig. 8(a), the dual pulse used in our experiment is a 100 Hz, 50% duty factor ($t_{ON} = t_{OFF}$ = 5 ms) signal. The pull-down voltage is −40 V and the hold-down voltage is −15 V. The pull-down pulse width (t_P) was varied as a parameter. Comparing with the 0 to −30 V square wave, the dual-pulse waveforms resulted in much less charging as expected. This trend is correctly predicted by the present model as shown in Fig. 8(b).

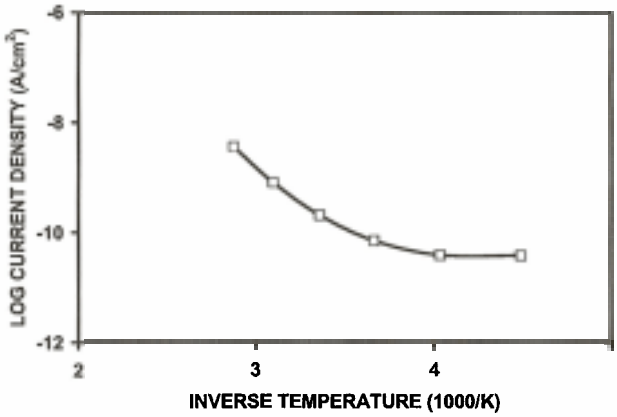

Fig. 9. Measured steady-state leakage current on the 500 x 500 μm² capacitor under -30 V control voltage. Measurement temperatures are -50, -25, 0, 25, 50, and 75°C.

VI. Discussion

The extracted charging and discharging time constants are independent of temperature as shown in Fig. 2. This indicates that the extracted time constants are not capture and emission times of the traps. Instead, the extracted time constants are characteristic of the diffusion-like charge redistribution process within the relatively thick dielectric. Once significant amount of charges are injected from the metal into the dielectric, they alter the field at the interface so that additional injection can occur only after the initial charges have sufficient time to diffuse inside the dielectric by trap hopping. The process is rather complicated and the time constants for the process showed no temperature dependence within our measurement temperature range.

The steady-state charge densities were found to exhibit Arrhenius behavior according to (4). Similar observations have been made on amorphous silicon thin-film transistors [12]-[14].

The injected charges are most likely distributed across the thickness of the dielectric. Since their collective effect on the actuation voltage can be approximated by a charge sheet, it greatly simplifies the model by using the charge-sheet assumption. Subtle difference between the MIM capacitor and the real switch may also be absorbed in h - an adjustment parameter in (5).

The dielectric and metal electrode used in the present switch resulted in unipolar charging from the bottom electrode independent of the sign of the control voltage. This greatly simplifies modeling and characterization of the charging effects making the charging model extracted from the MIM capacitor

readily applicable to the real switch. This will not be the case when different dielectrics and metals are used so that bipolar charging occurs through the top electrode and surface contamination and contact morphology become critical.

For the silicon dioxide used in this study, high leakage current is not necessarily desirable to reduce charge trapping. As shown in Fig. 9, the measured steady-state leakage current increases with increasing temperature. However, the steady-state charge densities and corresponding actuation-voltage shift also increase with temperature as shown in Fig. 1 and 3. Meanwhile, the spring constant and restoring force of the membrane decrease with increasing temperature. Therefore, the switch is more prone to charge-induced stiction when temperature increases. Conversely, lowering the temperature will increase the membrane spring constant while reducing charge injection, which will render a longer switch lifetime.

For RF MEMS capacitive switches whose lifetime is limited by dielectric charging, the present analysis shows that the number of operating cycles before failure is not a universal figure of merit. As shown by the modeled and measured data in Fig. 5 and 7, duty factor and peak voltage are critical acceleration factors. Therefore, control waveforms with high peak voltage, high duty factor, and low frequency can be used to accelerate failure. Conversely, control waveforms of low peak voltage, high frequency, and low duty factor may retard failure and result in improved lifetimes. In general, peak voltage, frequency, and duty factor must be specified to allow fair comparison of switch lifetimes.

VII. Conclusion

Acceleration factors of dielectric-charging effects in state-of-the-art RF MEMS capacitive switches were characterized and modeled. Based on the measured transient charging/discharging currents, a first-order charging model was extracted. The model was used to predict the amount of charge injected into the dielectric and the corresponding shift in actuation voltage. Charging effects were characterized and modeled under both DC and AC stress conditions. Agreement was obtained between the model prediction and experimental data. It was found that temperature, duty factor, and peak voltage were critical acceleration factors for charging effects whereas frequency had little effect on charging. Based on these acceleration effects, the present model can be used to design a favorable actuation waveform to minimize charging thus prolong the lifetime of RF MEMS capacitive switches. Conversely, the model can be used to design an efficient actuation waveform to accelerate charging and to validate the lifetimes obtained through accelerated life tests.

References

[1] C. L. Goldsmith, Z. Yao, S. Eshelman, and D. Denniston, "Performance of low-loss RF MEMS capacitive switches," *IEEE Microwave Guided Wave Lett.*, vol. 8, pp. 269-271, Aug. 1998.

[2] A. Malczewski, S. Eshelman, B. Pillans, J. Ehmke, and C. L. Goldsmith, "X-band RF MEMS phase shifters for phased array applications," *IEEE Microwave Guided Wave Lett.*, vol. 9, pp. 517-519, Dec. 1999.

[3] D. Peroulis, S. Pacheco, K. Sarabandi, and L. P. B. Katehi, "MEMS devices for high isolation switching and tunable filtering," in *IEEE MTT-S Int. Microwave Symp. Dig.*, vol. 2, June 2000, pp. 1217-1220.

[4] G. M. Rebeiz, G.-L. Tan, and J. S. Hayden, "RF-MEMS phase shifters: design and applications," *IEEE Microwave Mag.*, vol. 3, pp. 72-81, June 2002.

[5] C. L. Goldsmith, J. Ehmke, A. Malczewski, B. Pillans, S. Eshelman, Z. Yao, J. Brank, and M. Eberly, "Lifetime characterization of capacitive RF MEMS switches," in *IEEE MTT-S Int. Microwave Symp. Dig.*, vol. 1, June 2001, pp. 227-230.

[6] X. Yuan, S. V. Cherepko, J. C. M. Hwang, C. L. Goldsmith, C. Nordquist, and C. Dyck, "Initial observation and analysis of dielectric-charging effects on RF MEMS capacitive switches," in *IEEE MTT-S Int. Microwave Symp. Dig.*, vol. 3, June 2004, pp. 1943-1946.

[7] J. R. Reid and R. T. Webster, "Measurements of charging in capacitive microelectromechanical switches," *Electron. Lett.*, vol. 38, no. 24, pp. 1544-1545, Nov. 2002.

[8] W. M. van Spengen, R. Puers, R. Mertens, and I. De Wolf, "Experimental characterization of stiction due to charging in RF MEMS," *in IEDM Tech. Dig.*, Dec. 2002, pp. 901-904.

[9] W. M. van Spengen, R. Puers, R. Mertens, and I. De Wolf, "A comprehensive model to predict the charging and reliability of capacitive RF MEMS switches," *J. Micromech. Microeng.*, vol. 14, no. 4, pp. 514-521, Jan. 2004.

[10] X. Yuan, J. C. M. Hwang, D. Forehand, and C. L. Goldsmith, "Modeling and characterization of dielectric-charging effects in RF MEMS capacitive switches," in *IEEE MTT-S Int. Microwave Symp. Dig.*, June 2005, pp. 753-756

[11] X. Yuan, J. C. M. Hwang, D. Forehand, and C. L. Goldsmith, "Temperature acceleration of dielectric-charging effects in RF MEMS capacitive switches," to appear in *IEEE MTT-S Int. Microwave Symp. Dig.*, June 2006.

[12] S. W. Wright and J. C. Anderson, "Trapping centers in sputtered SiO_2 films," *Thin Solid Films*, vol. 62, pp. 89-96, 1979.

[13] M. J. Powell, "Charge trapping instabilities in amorphous silicon-silicon nitride thin-film transistors," *Appl. Phys. Lett.*, vol. 43, pp. 597-599, Sep. 1983.

[14] A. V. Gelatos and J. Kanicki, "Bias stress-induced instabilities in amorphous silicon nitride/hydrogenated amorphous silicon structures: Is the "carrier-induced defect creation" model correct?" *Appl. Phys. Lett.*, vol. 57, pp. 1197-1199, Sep. 1990.